ATLAS internal note
January 11, 2000

Studies of Hard Diffraction in ATLAS

Giuseppe Battistoni[a] and Stefan Tapprogge[b]

a) INFN Milano
b) CERN - EP Division

Abstract

This note summarizes the results of first studies of hard single diffraction and hard central diffraction in the LHC environment with the ATLAS detector. The studies have concentrated on the expected cross-sections and first attempts have been made to investigate the sensitivity of some observables to the partonic structure.

Using the PHOJET Monte Carlo, samples of non-diffractive, single diffractive and double diffractive events have been generated. The tagging of diffractive events by requiring a leading proton and properties of the final state via jet production have been investigated with the aim of getting information on the partonic structure of the exchange (the Pomeron). Both for single hard diffractive scattering and central hard diffractive scattering, cross-sections for various final state requirements are presented, together with distributions derived from jet properties which exhibit sensitivity to the underlying partonic structure. An extensive list of topics for further studies is provided.

1 Introduction

This note summarizes the results of first studies of hard single diffraction and hard central diffraction in the LHC environment with the ATLAS detector. The studies have concentrated on the expected cross-sections and first attempts have been made to investigate the sensitivity of some obvservables to the partonic structure.

Using the PHOJET Monte Carlo [1], samples of non-diffractive, single diffractive and double diffractive events have been generated. The tagging of diffractive events by requiring a leading proton and properties of the final state via jet production have been investigated with the aim of getting information on the partonic structure of the exchange (the Pomeron).

The note is structured as follows. Section 2 contains a description of the kinematic variables used to describe diffractive scattering. In Section 3, the PHOJET Monte Carlo program used in these studies is described, followed by a description of the selection for diffractive physics to be used at LHC. Section 4 discusses issues related to the partonic structure and is followed by a discussion of the results for hard single and hard central diffractive scattering. The note concludes with a list of issues for further studies.

2 Diffraction and related kinematic variables

Landau and his collaborators, in the fifties, introduced the term diffraction in high energy physics in complete analogy with the well known phenomenon in Optics that occurs when light interacts with obstacles or holes whose dimensions are of the order of the electromagnetic radiation wavelength. The interaction of a hadron could be thought of as the absorption of its wave function caused by the different channels open at high energy and consequently the name diffraction seems to be intuitive. The prediction coming from the optical analogy is a series of diffractive maxima and minima, entirely similar to the case in Optics, and have been clearly observed in several experiments.

In the specific field of particle physics, diffraction is said to be the dominant process of scattering at high energy if no quantum numbers are exchanged between the colliding particles. In other words, diffraction dominates asymptotically as soon as the particles in the final state have the same quantum numbers as the incident ones. This sort of definition of diffraction clearly includes, for two-body scattering, three cases: elastic scattering, single diffraction and double diffraction. In the first process the outgoing particles are exactly the same as the incident ones. In the second case, one incident particle goes out unmodified while the second one gives rise to a resonance, or to a bunch of final-state particles, with total quantum numbers coincident with its own ones. Finally, when double diffraction occurs, each incident particle gives rise to a resonance, or to a bunch of final-state particles, with the same quantum numbers of the initial ones.

For elastic scattering $pp \to pp$, the two protons exchange transverse momentum only. The squared momentum transfer t is given by the expression $t = (P - P')^2$, where P (P') is the four-momentum of one of the protons before (after) scattering. In the limit $-t \ll s$, their longitudinal momentum $x_L = x_F$ remains constant, i.e. the outgoing protons have $x_F = 1$.

In the case of single diffractive scattering $pp \to pX$, a second variable is available, as the longitudinal momentum of the quasi-elastically scattered proton can be less than the

beam momentum $x_F < 1$. These interactions can be thought as mediated by the exchange of a colorless object which carries a fraction ξ of the incoming proton momentum, where $x_F = 1 - \xi$. Again in the limit $-t \ll s$, the invariant mass M_X of the diffractive system X is given by $M_X = \sqrt{\xi \cdot s}$. For central diffractive scattering $pp \to pXp$, both protons scatter quasi-elastically ($x_{F1,2} < 1$), the invariant mass M_X of the system X is given by $M_X = \sqrt{\xi_1 \xi_2 \cdot s}$. In the picture of the Regge theory, such colorless object is the Pomeron.

Trying to connect the Pomeron with the language and understanding of QCD, one can imagine it as a colour singlet combination of partons such as the simplest picture of a pair of gluons proposed by Low and Nussinov [2]. Two-gluon exchange is compatible with all soft phenomenology except that this simple model gives a constant, not a rising, total cross-section. Clearly in order to analyze the parton content of pomeron, a hard or high-momentum transfer interaction analogous to the one used to find the quark-gluon content of the proton is necessary. This kind of processes is called hard diffraction making reference to the hard scale that ultimately allows the pertubative description.

The main point to be solved is related to the precise relation between hard and soft diffraction. In order to study the pomeron parton content, small distances and high-momentum transfer are necessary, while the natural environment of the soft Pomeron is at large distances and low-momentum transfer. In other words, the clear notion of a Pomeron is still missing.

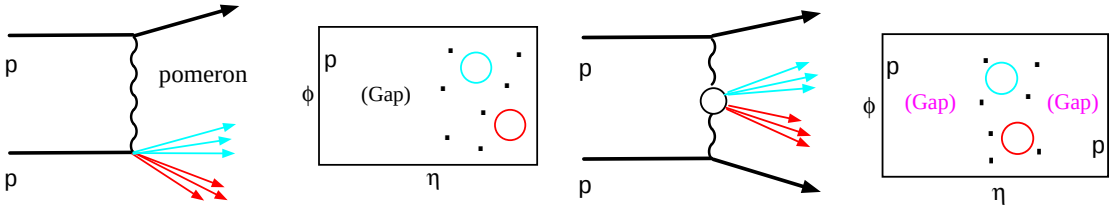

Figure 1: Sketch of hard single diffractive scattering (left) and hard central diffractive scattering (right), as well as the resulting final state distribution in the $\eta - \phi$ space.

Figure 1 shows in the left part the case of hard single diffractive scattering, where one proton is scattered quasi-elastically and 'emits' a Pomeron. The inelastic interaction of the Pomeron with the second proton leads to a final state with two jets. In the $\eta - \phi$ space, the quasi-elastically scattered proton (leading proton) is separated from the final state (containing two jets) of the inelastic reaction by a gap in rapidity. The right part of this figure shows the case of hard central diffractive scattering, where both protons scatter quasi-elastically. The inelastic interaction takes place between the two Pomerons 'emitted' from the two protons. In $\eta - \phi$ space there are now two large rapidity gaps, separating the final state (with two jets) from both leading protons. The study of hard diffractive events has been stimulated by the experimental findings at HERA, first, and later at TEVATRON (see Section 3 and Appendices B and C). The topology of these final states is different from those of inelastic minimum bias events, where an exchange of color quantum number occurs between the protons, and where no large rapidity gaps are produced.

In section 5 more variables are described for hard diffractive scattering, which are related to the partonic structure.

3 The PHOJET Monte Carlo program

The simulation of hard diffractive events requires specialized Monte Carlo codes, which are in general different from those adopted for the production of minimum bias events. One of the most interesting models is PHOJET, which is a first attempt to built a Monte Carlo model for multiparticle production which includes multiple soft and hard interactions between the constituents of the projectile and target, as well as multiple interactions in the pomeron-projectile, pomeron-target, and pomeron-pomeron scattering subprocesses. It accounts for both non–diffractive and diffractive interactions.

The Monte Carlo implementation of PHOJET is based on the "two-component Dual Parton Model". This model combines results obtained within Regge theory, Gribov's reggeon calculus [3, 4] and Abramowski-Gribov-Kancheli (AGK) cutting rules [5] with perturbative QCD predictions for hard interaction processes (see for example [6–8], a review is given in [9]).

The Dual Parton Model (DPM) describes high-mass diffractive hadron production in terms of enhanced graphs like the triple-pomeron graph [10]. As already discussed in [11], within this approach, diffractive processes can be considered as collisions of a color neutral object, the pomeron, with hadrons, photons or other pomerons. However, it is important to note that the pomeron cannot be considered as an ordinary hadron. It is only a theoretical object providing an effective description of the important degrees of freedom of a certain sum of Feynman diagrams in the Regge limit (e.g. the available c.m. energy is large compared to the momentum transfer characterizing the scattering process). In this sense, pomeron-hadron or pomeron-pomeron interactions can only be discussed in the framework of collisions of other particles like hadrons or photons. In this model, high-mass diffraction dissociation exhibits properties similar to hadron production in non-diffractive hadronic collisions at high energies. Experimental data on diffraction support this idea, on the basis that the mass of the diffractively produced system corresponds to the collision energy in non-diffractive interactions [12, 13]. The striking similarities between diffractive and non-diffractive multiparticle production suggest that multiple soft and hard interactions may also play an important role in high-mass diffraction dissociation. Hard diffraction is described using leading-order QCD matrix elements together with a parton distribution function for the pomeron and pomeron-flux factorization (see below).

Additional mechanisms have to be invoked to reproduce the phenomenology of new observed classes of events, like the two jet events with a large rapidity gap between the jets, as those observed at TEVATRON [14,15]: at least one pomeron has a large virtuality and standard Regge phenomenology cannot be applied. Therefore, one has to introduce a new kind of process like soft color reconnection (SCR) [16–20] or perturbative gluon-ladder exchange [21, 22]. The PHOJET model includes also SCR in hard scattering processes similar to what proposed in ref. [20]. More details on the model can be found in Appendix A.

It has been already pointed out that the model for particle production in pomeron–hadron/photon collisions and pomeron–pomeron collisions has the same structure characterized by multiple soft collisions and multiple minijets like models for hadron production in non-diffractive hadron–hadron collisions. Therefore, we expect that the main differences in the hard component, when comparing the different channels, are due to the differences between the pomeron and hadron structure functions and due to the existence or non-existence of a direct pomeron–quark coupling.

The differences in the parton structure functions of protons, photons and pomerons lead to quite different energy dependences of the hard cross sections. In all processes where pomerons are involved (single diffraction and central diffraction), hard processes become important already at lower energies than in hadron-hadron collisions. For pomeron–pomeron scattering at low energy the hard cross section is about a factor 100 bigger than that of p–$\bar{p}$ collisions. At high energies the opposite happens, the hard cross sections in all processes where pomerons are involved rise less steeply with energy than in purely hadronic or photonic processes. The reason for this is the different low-x behavior of the parameterization of the structure functions used. However, nothing is known at present from experiment about the low-x behavior of the pomeron structure function. More details on the comparison between p–p and γ–γ reactions can be found in Appendix B.

3.1 Benchmarking with Experimental Data

As will be shown below and in Appendix C, the PHOJET model is able to describe data on diffractive hadron production from the CERN and FERMILAB colliders and from the HERA lepton-proton collider. In this section some of the results obtained at the Tevatron collider which have been used to validate the PHOJET model are reviewed. More comparisons with other data can be found in Appendix C. Plots and numbers in this section are taken from ref. [61].

3.1.1 Single diffraction and central diffraction at TEVATRON

In Figs. 2 and 3 examples of cross sections calculated using PHOJET at the TEVATRON energy are shown. The distributions are mass distributions in single and central diffraction (Fig. 2) and jet pseudorapidity distributions in single and central diffraction using $E_\perp$ thresholds of 5 and 15 GeV (Fig. 3.a and 3.b). In all figures three different cuts for the Feynman-x of the diffracted nucleons are considered: $x_F > 0.9$, 0.95 and 0.97. It is obvious that all distributions and cross sections depend strongly on these cuts.

One of the results obtained by the D0 Collaboration is the ratio of double–pomeron exchange (DPE, detected by a large rapidity gap signature)[1] to non–diffractive (ND) dijet events [62]:

$$\left(\frac{\sigma(\mathrm{DPE})}{\sigma(\mathrm{ND})}\right)_{E_\perp^{\mathrm{jet}}>15\mathrm{GeV}} \approx 10^{-6} \tag{1}$$

Within the PHOJET model one gets the following total cross sections:

Non-diffractive interactions (ND): $\sigma(\mathrm{ND}) = 45.2$ mb,
Both-side single diffraction dissociation (SD): $\sigma(\mathrm{SD}) = 11.2$ mb,
Central diffraction (CD): $\sigma(\mathrm{CD}) = 0.64$ mb.

From these cross sections, together with Figs. like 3, and requiring $E_\perp^{\mathrm{jet}}$ larger than 15 GeV, the following ratios are obtained:

(CD)/(ND)$\approx 2 \times 10^{-6}$,
(SD)/(ND)$\approx 4 \times 10^{-3}$,
(CD)/(SD)$\approx 0.5 \times 10^{-3}$.

Despite the fact that no experimental acceptance has been considered for these PHOJET results it is interesting to find the (CD)/(ND) ratio so close to the D0 value given above.

[1] In [62] the term double–pomeron exchange is used instead of central diffraction.

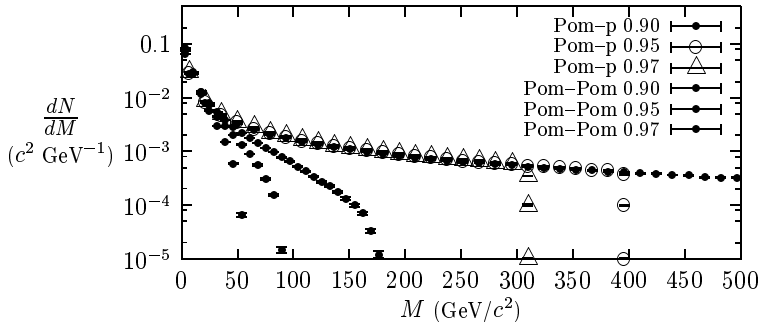

Figure 2: Distribution of the diffractive mass in single diffraction dissociation (pomeron–proton) and central diffraction (pomeron–pomeron) at TEVATRON ($\sqrt{s} = 1.8$ TeV) for three different cuts of the Feynman-x of the diffractive nucleons.

3.1.2 Diffractive dijet production at TEVATRON

Data on dijet production in single diffraction dissociation using a large rapidity gap trigger were published by the CDF Collaboration [63]. Same side ($\eta^{\rm jet1} \times \eta^{\rm jet2} > 0$) dijets were selected with $E_\perp^{\rm jet} > 20$ GeV in the jet pseudorapidity window $1.8 < |\eta^{\rm jet}| < 3.5$. The gap trigger did demand no charged hadrons in the range $3.2 < |\eta| < 5.9$ opposite to the jets and no calorimeter hit above 1.5 GeV in the range $2.4 < |\eta| < 4.2$ opposite to the jets. The ratio of dijet events with gap (JJg) to dijets without gap (JJ) was found to be

$$R_{\rm JJg-CDF} = \frac{\rm (JJg)}{\rm (JJ)} = (0.75 \pm 0.05 \pm 0.09)\% \ . \tag{2}$$

A test using PHOJET was performed producing good statistics only for $E_\perp^{\rm jet} > 10$ GeV when using the CDF pseudorapidity restrictions. The following cross sections are obtained: $\sigma_{\rm JJ} = 50.4$ μb and $\sigma_{\rm JJg} = 0.107$ μb. This gives the ratio $R_{\rm JJg-PHOJET} = 0.21\%$. There are two possible reasons for this ratio being smaller than the one found by CDF: (i) the different $E_\perp$ cut and (ii) the CKMT pomeron structure functions [31, 32] used in the calculation might not contain enough hard gluons.

In Fig.4.a the $E_\perp^{\rm jet}$ distributions calculated from PHOJET for the JJ and JJg events are presented. Within the statistics of the Monte Carlo calculation both distributions seem to have the same shape.

In Fig.4.b the $\phi^{\rm jet1} - \phi^{\rm jet2}$ distributions for the JJ and JJg events are shown. Again within the statistics both distributions seem to be quite similar. However, in the JJ events additional jet-pairs are found more often than in the JJg events. Therefore, a stronger correlation of the two jets in the JJg events is expected.

3.1.3 Dijet production by color–singlet exchange at TEVATRON

Only data on dijet production by color–singlet exchange published by the CDF and D0 Collaborations from refs. [14, 15] are considered here.

D0 [14] finds opposite side ($\eta^{\rm jet1} \times \eta^{\rm jet2} < 0$) dijets with $E_\perp^{\rm jet} > 30$ GeV and $|\eta^{\rm jet}| > 2$. The pseudorapidity gap is at $|\eta| < 1.3$. The fraction of JgJ events is found to be

$$R_{\rm JgJ-D0} = \frac{\rm (JgJ)}{\rm (JJ)} = (1.07 \pm 0.10^{+0.25}_{-0.13})\% \tag{3}$$

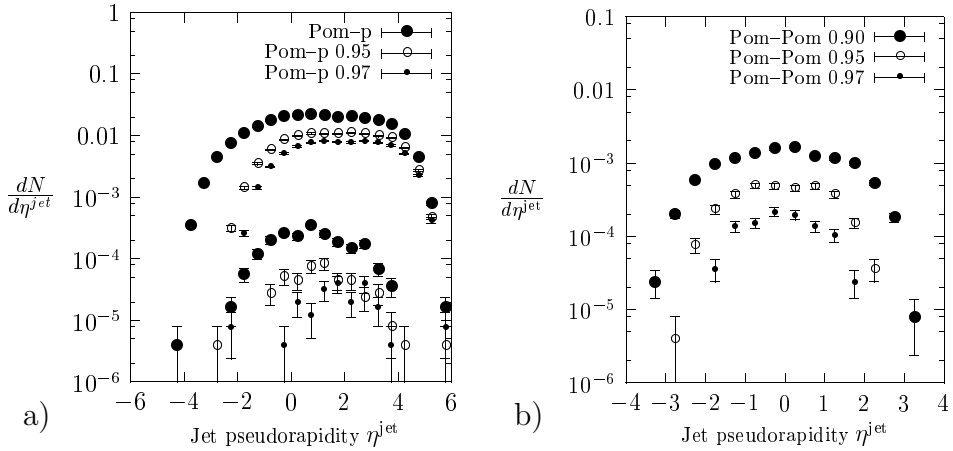

Figure 3: (a) Pseudorapidity distribution of jets with $E_\perp$ larger than 5 GeV and 15 GeV in (one side) single diffraction (Pom–p) at TEVATRON for three different cuts of the Feynman-x of the diffractive nucleon. The upper curves with the same symbols are for $E_\perp = 5$ GeV, the lower curves are for $E_\perp = 15$ GeV. (b) Pseudorapidity distribution of jets with $E_\perp$ larger than 5 GeV in central diffraction (Pom–Pom) at TEVATRON for three different cuts of the Feynman-x of the diffractive nucleons.

CDF [15] uses opposite side jets with $E_\perp^{\rm jet} > 20$ GeV and $3.5 > |\eta^{\rm jet}| > 1.8$ with a gap at $|\eta| < 1.0$. The gap fraction is found to be

$$R_{\rm JgJ-CDF} = \frac{\rm (JgJ)}{\rm (JJ)} = (1.13 \pm 0.12 \pm 0.11)\% \ . \tag{4}$$

Furthermore, the jets are found to be back–to–back correlated in $\phi^{\rm jet1} - \phi^{\rm jet2}$.

In PHOJET using SCR, applying the D0 trigger

$$R_{\rm JgJ-PHOJET-D0} = \frac{\rm (JgJ)}{\rm (JJ)} = 0.43\% \ . \tag{5}$$

Here 0.1% background JgJ events with only an accidental gap was subtracted, as it was determined in a run without the use of SCR.

With the CDF trigger instead, it is found

$$R_{\rm JgJ-PHOJET-CDF} = \frac{\rm (JgJ)}{\rm (JJ)} = 0.50\% \tag{6}$$

where 0.5% background JgJ events had to be subtracted.

In the PHOJET Monte Carlo the hard scattering events can be subdivided into g–g, g–q and q–q scatterings. In Fig.5 the fractions of g–g, g–q and q–q events are plotted using the D0 and CFD trigger, for JJ events (without gap trigger), JgJ events obtained with SCR and background JgJ events (obtained without SCR). In both cases q–q scattering dominates the JgJ events, but g–q and g–g scattering contributes also. For the q–q events the fraction of JgJ events due to SCR (background subtracted) is always smaller than 1% of the q–q scatterings without gap.

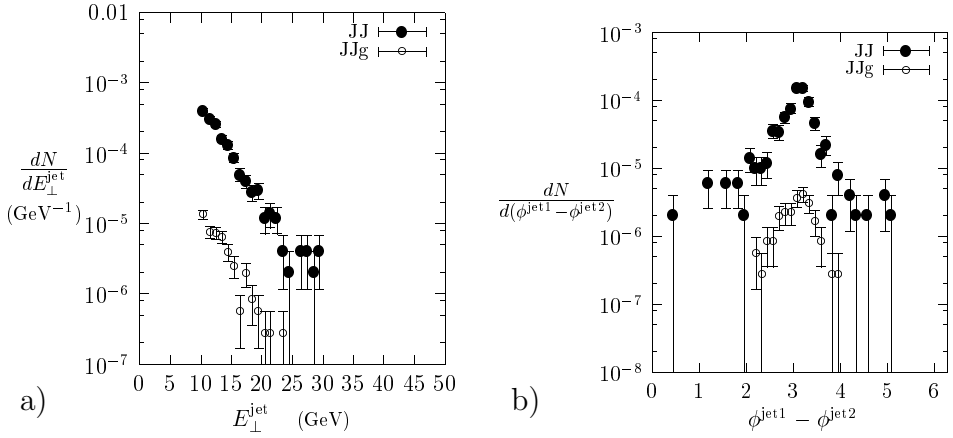

Figure 4: (a) $E_\perp^{\rm jet}$ distributions in JJ and JJg events obtained in PHOJET using the CDF triggers. (b) $\phi^{\rm jet1}$ - $\phi^{\rm jet2}$ distributions in JJ and JJg events obtained with PHOJET using the CDF trigger.

In Fig. 6.a the $\phi^{\rm jet1} - \phi^{\rm jet2}$ distribution calculated with PHOJET is presented for the JJ and JgJ events for the CDF trigger together with the corresponding distribution published by CDF [15]. All distributions are rather similar. However, with bigger statistics a stronger correlation in the JgJ events is expected, because additional jets are much less frequent than in the JJ events. In Fig. 6.b the calculated $E_\perp^{\rm jet}$ distribution is presented. Within the statistics of the Monte Carlo runs no differences between the distributions corresponding to the JJ and JgJ events can be appreciated.

The change of $R_{\rm JgJ}$ with the $E_\perp^{\rm jet}$ was studied by the D0 Collaboration [37]. A modest rise of the color singlet fraction with $E_\perp^{\rm jet}$ was found. In Fig. 7 PHOJET results on $R_{\rm JgJ}$ are compared with these preliminary data. The PHOJET predictions exhibit a flat $E_\perp^{\rm jet}$ dependence being still compatible with the data [2]. The D0 Collaboration [37] also found $R_{\rm JgJ}$ at $\sqrt{s} = 630$ GeV to be a factor 2.6$\pm$ 0.6 larger than at $\sqrt{s} = 1.8$ TeV. The ratio of $R_{\rm JgJ}$ at these energies calculated with PHOJET is consistent with the data, see Fig. 7.

4 Selection of diffractive events

The selection of diffractive events can either rely on the observation of one or two leading protons or on the observation of large rapidity gaps (regions without particle production) in the final state. In the following, only the selection using the detection of one or two leading protons is used. More studies are needed to investigate a possible selection using the large rapidity gap signature. With this method however only an upper limit on the mass of the forward going colour-neutral system can be given – since it is not possible to prove that the leading system is a proton. Thus, a contamination from events where the proton dissociates into a low mass system (or into an excited baryon state) is expected.

In the absence of a detailed calculation of the acceptance in (ξ, t) for a configuration of Roman Pots as suggested by the TOTEM collaboration [67], the following reasonable assumptions have been made. A leading proton is assumed to be detectable (with an

[2]Very recent data of the CDF Collaboration [15] on a similar ratio show also a flat $E_\perp^{\rm jet}$ dependence

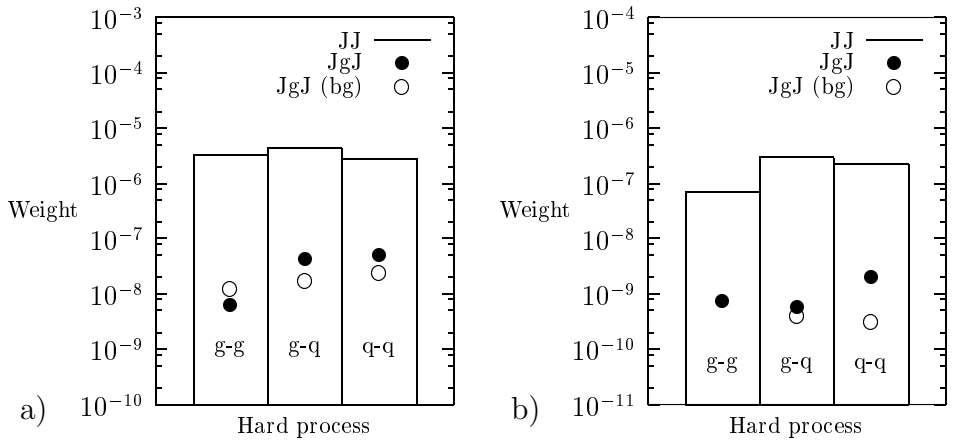

Figure 5: (a) Monte Carlo predictions for the fractions of g–g, g–q and q–q hard scatterings in the JJ events (without gap trigger), JgJ events obtained with SCR and background (bg) JgJ events (obtained without SCR) for the CDF trigger. (b) Same as in (a) but for the D0 trigger.

efficiency of 100 %, which is larger than expected) in the kinematic range $x_F > 0.9$ and $0.01 < |t| < 1$ GeV^2.

5 Probing the partonic structure

The partonic structure in diffractive scattering can be probed in a similar manner to the study of the partonic structure of the proton. In the context of diffractive Deep Inelastic Scattering ($\ell N \to \ell X Y$), it is customary to define *diffractive structure functions*, in analogy with the ordinary ones, through the expression of the corresponding cross section

$$\frac{d^4\sigma(\ell N \to \ell X Y)}{dx\, dQ^2\, d\xi\, dt} = \frac{4\pi\alpha_{em}^2}{x Q^4}\left[\left(1 - y + \frac{y^2}{2}\right) F_2^{D(4)} - \frac{y^2}{2} F_L^{D(4)}\right] \tag{7}$$

where

$$F_2^{D(4)} = F_T^{D(4)} + F_L^{D(4)}$$

and where ξ is the momentum fraction carried by the Pomeron. The superscript "(4)" implies that the structure functions F^D depend on four kinematic variables, which usually are chosen to be: ξ, t, β and Q^2. In the most naive Regge inspired approach, the diffractive structure function is assumed to be given by the product of the probability $f_{I\!P/p}(\xi, t)$ to find a pomeron in the incoming proton, which only depends on the variables ξ and t, and a *pomeron structure function* $F_2^{I\!P}(\beta, Q^2)$, given by parton densities which are assumed to behave according to Altarelli-Parisi evolution equations and factorize as ordinary parton distributions. This hypothesis is called "factorization". More details on factorization and its validity in perturbative QCD can be found in [38].

Using high p_T final state objects like jets, W and Z bosons, Drell-Yan pairs, photons or heavy quarks, information about the gluonic and quarkonic content of the reaction can be obtained.

In case of hard single diffractive scattering, the momentum fraction β of a parton entering the hard scattering can be calculated from the properties of the two jets produced

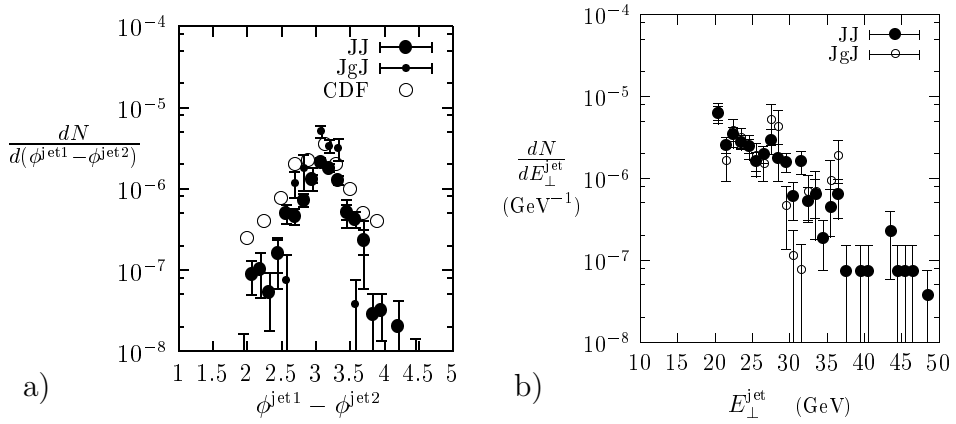

Figure 6: (a) The $\phi^{\rm jet1} - \phi^{\rm jet2}$ distributions corresponding to the CDF trigger [15]. (b) The $E_\perp^{\rm jet}$ distributions corresponding to the CDF trigger. In both cases the distributions are normalized one to each other.

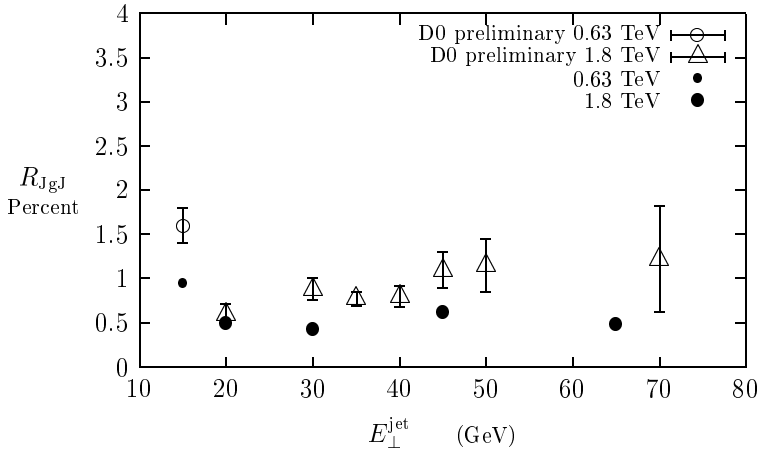

Figure 7: The change of $R_{\rm JgJ}$ with $E_\perp^{\rm jet}$. Preliminary data from the D0 Collaboration [37] are compared to the PHOJET results (filled circles) obtained with SCR.

($E_{T\ 1,2}$ and $\eta_{1,2}$) as follows:

$$\beta = \frac{E_{T\ 1} e^{-\eta_1} + E_{T\ 2} e^{-\eta_2}}{2\sqrt{\xi} P_{beam}}, \tag{8}$$

where ξ is assumed to be determined from the measurement of the scattered leading proton (beam momentum P_{beam}). However it has to be remembered that this momentum fraction cannot always be equated with the momentum fraction x of a parton out of the Pomeron.

For the studies presented here, it has been assumed that hard scattering factorization holds and that one can define parton densities of the Pomeron. To estimate the sensitivity of several observables to the parton densities, three different parton distribution sets for the Pomeron have been used:

soft gluon:

the Pomeron is assumed to consist only of gluons, whose distribution is soft. This means that the distribution in the fractional momentum x (relative to the Pomeron momentum) follows the functional form $x \cdot g(x) \propto (1-x)^5$.

hard gluon:

the Pomeron is assumed to consist only of gluons, whose distribution is hard. This means that the distribution in the fractional momentum x (relative to the Pomeron momentum) follows the functional form $x \cdot g(x) \propto x \cdot (1-x)$.

CKMT [31, 32]:

in this case the Pomeron is composed out of quarks and gluons, which evolve according to the DGLAP equations. This parametrisation leads to a hard gluon component, too.

6 Simulation of single hard diffractive di–jet production

Using PHOJET, we have simulated (at particle level) single hard diffractive events at LHC, implementing trigger conditions for the di–jet production in this channel, following the experience of the measurement performed by the CDF collaboration [64]. There they used a a sample of same-side ($\eta_1 \times \eta_2 > 0$) di–jet events with a minimum transverse energy of 20 GeV for each jet. Using the information on charged particle from the tracking detectors, on calorimeter towers and hits in the scintillators of the beam-beam counters, multiplicity distribution on the side opposite to the jet system were studied and a clear excess of events with zero multiplicity was observed. The fraction of the diffractive di–jet events with respect to the non-diffractive ones was determined to be ($0.75 \pm 0.05 \pm 0.099$) [64]. A further study by CDF [65] used a sample of events at 630 GeV and at 1800 GeV, where a leading anti-proton ($0.04 < x_F < 0.095$ and $|t| < 1$ (GeV/c)^2) has been measured. This allows tagging of colourless t-channel exchange in the kinematic region where Pomeron exchange should dominate. In both samples, large E_T jet pairs are observed, with a distribution of transverse energy similar (with a slightly steeper slope) to the one of jets in non-diffractive events.

The shape of the beta distribution gives information about the partonic structure of the Pomeron.

In the study presented here, jets have been searched with a jet–cone algorithm [66] applied to charged particles having $P_\perp > 0.3$ GeV/c produced in the region defined by $|\eta| < 3.2$. The cone radius in the $\phi - \eta$ space has been set to 1.0, with a tranverse energy threshold for a jet seed of 1.0 GeV and a jet E_T threshold of 3.0 GeV.

The resulting jets have been sorted according to their transverse energy, and a threshold of 10 GeV has been applied. In fact, triggering of events with a hard diffractive interaction requires low transverse energy thresholds for the jets, due to the small invariant mass of the diffractive system.

It is expected that the non-diffractive contribution has a cross-section which is almost two orders of magnitude larger than the single diffractive contribution. The rate for a di–jet trigger with low energy threshold would completely saturate the bandwidth of the trigger system. It can however be reduced by demanding the detection of a leading proton.

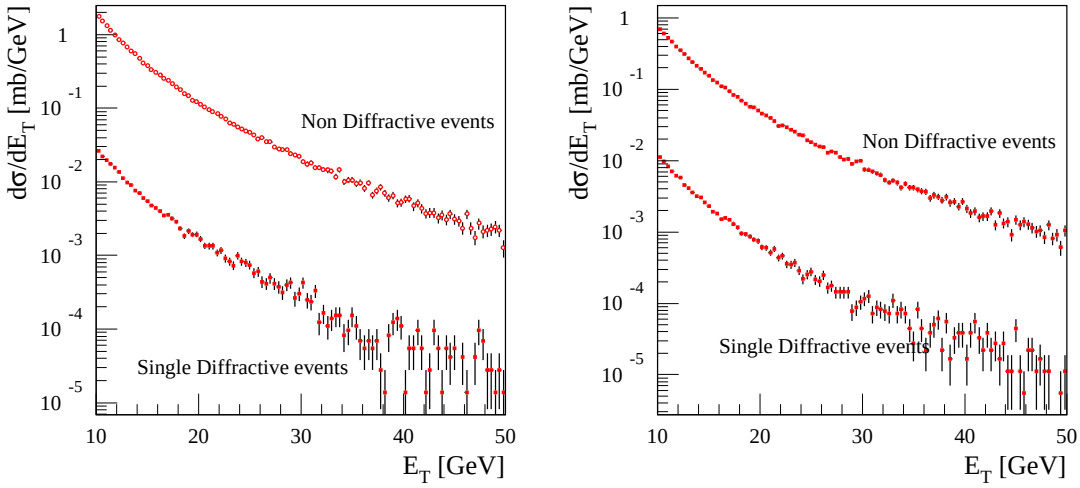

Figure 8: Cross-section for di–jet production ($|\eta_{jet}| < 3.2$) as a function of the jet transverse energy for non-diffractive and single diffractive events, obtained from the PHOJET Monte Carlo model. Left side: hard pomeron. Right side: soft pomeron.

We have therefore asked for an additional leading proton with $x_F > 0.9$ and $0.01 < |t| < 1$ $(\mathrm{GeV/c})^2$ being tagged in the direction opposed to that of the two jets.

We have generated $2{\cdot}10^6$ events at $\sqrt{s}$= 14 TeV with PHOJET selecting non–diffractive events, and then we performed the generation (with the same number of collisions) for single diffractive events. In both cases we have repeated the study for two different choices of parton distribution functions for the Pomeron quoted in the previous section: the "soft gluon" and the "hard gluon" distributions.

In summary, we obtain the following numbers, which are shown in Tab. 1.

Event generation	σ (mbarn)	Events with $\geq$ 2 jets	Events with $\geq$ 2 jets and $E_T \geq$ 10 GeV	Events with $\geq$ 2 jets and $E_T \geq$ 10 GeV and leading proton tag
single diffr., soft	5.53	137821	3795	2097
single diffr., hard	5.53	48068	2746	2011
non–diffr., soft	67.74	766939	41507	61
non–diffr., hard	67.74	767073	41619	51

Table 1: Simulated number of events after various cuts for single diffractive and non-diffractive scattering.

In Fig. 8 the expected cross-sections for di–jet production with $E_T > 10$ GeV and $|\eta| < 3.2$ are shown as a function of the minimum transverse energy. Fig. 9 shows the visible cross-section for the production of two jets with the same cuts as for Fig. 8, but with the additional requirement of a leading proton. The visible non-diffractive cross-section is now smaller by about one order of magnitude than the single diffractive cross-section.

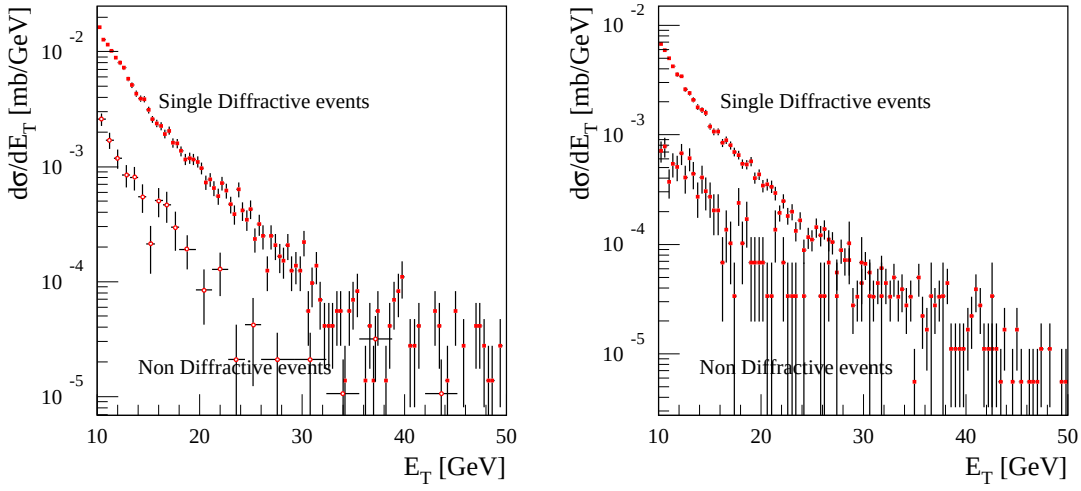

Figure 9: Visible cross-section for di–jet production ($|\eta_{jet}| < 3.2$) as a function of the jet transverse energy for non-diffractive and single diffractive events, when the detection of a leading proton is required, as obtained from the PHOJET Monte Carlo model. Left side: hard pomeron. Right side: soft pomeron.

.

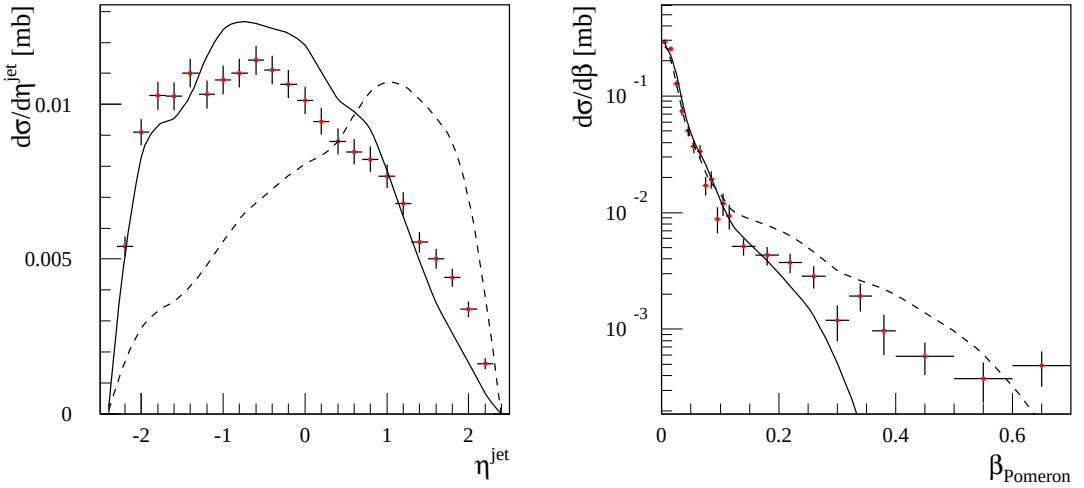

Figure 10: Left side: Visible cross-section for di–jet production ($|\eta_{jet}| < 3.2$) as a function of the jet pseudo-rapidity η^{jet} for single diffractive events. Right side: visible cross-section for di–jet production ($|\eta_{jet}| < 3.2$) as a function of the parton momentum fraction $\beta_{Pomeron}$ for single diffractive events. In both cases the detection of a leading proton is required, as obtained from the PHOJET Monte Carlo model. Three parametrisations of the Pomeron partonic structure have been used: CKMT (points), "hard gluon" (dashed line) and "soft gluon" (solid line).

.

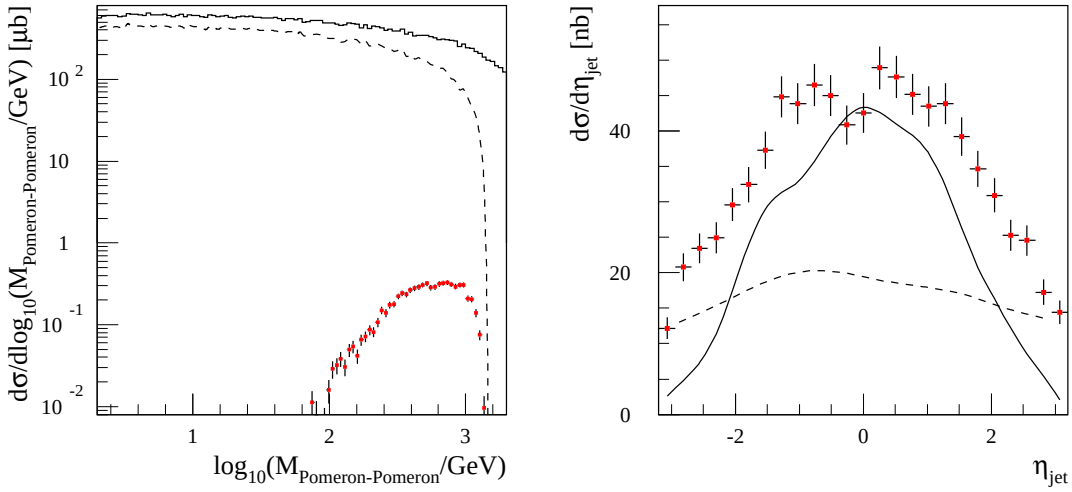

Figure 11: Cross-section for central diffraction as a function of the invariant mass $M_{Pomeron-Pomeron}$ of the diffractive system (left side), for various cuts: no final state requirements (solid line), two leading protons (dashed line) and in addition at least two jets (points). Cross-section for central diffraction with di-jet production as a function of the pseudo-rapidity η_{jet} of the jet (right side), where the detection of two leading protons is required, as obtained from the PHOJET Monte Carlo model. The three parametrisations of the Pomeron partonic structure have been used: CKMT (points), 'hard gluon' (dashed line) and 'soft gluon' (solid line).

.

The left part of Fig. 10 shows the cross-section for single diffractive events (tagged with a leading proton) with at least two jets with $E_T > 10$ GeV and $|\eta| < 3.2$ as a function of the pseudorapidity of the two leading jets. Most likely the actual minimum transverse momentum of the jets will be larger than 10 GeV, firstly due to constraints on the trigger rate and secondly due to the challenges in reconstructing jets with small transverse energy. Three different assumptions on the partonic structure of the Pomeron have been used: the CKMT parametrisation (shown as points), the "soft gluon" (solid line) and the "hard gluon" (dashed line). Between the last assumption and the first two, a very different shape is observed. Measuring the pseudorapidities of the two jets and their transverse energy allows determination of the momentum fractions β of the partons in the hard scattering (assuming hard scattering factorisation). The right part of Fig. 10 indicates the cross-section for single diffractive di-jet production as a function of β, for the same three assumptions on the partonic structure of the Pomeron. The differences between the assumptions are not as pronounced as in the case of the jet pseudorapidity distribution. More detailed studies are needed to assess the accessible kinematic range.

7 Results on hard central diffractive scattering

The selection of central diffractive scattering requires two leading protons, both with $x_F > 0.9$ and $0.01 < |t| < 1$ GeV^2.

In figure 11 (left part) the expected cross-section for central diffraction is shown

as a function of the invariant mass $M_{Pomeron-Pomeron}$ of the diffractive system. Three different cases are displayed: (a) no requirements on the detection of leading protons (solid histogram), (b) requiring two leading protons, according to the selection mentioned above (dashed line), and (c) requiring in addition at least two jets with $|\eta_{jet}| < 3.2$ and $E_T > 10$ GeV. As can be seen, at LHC a wide range in the mass of the diffractive system is covered, reaching up to values of more than 1 TeV. The selection of two leading protons leads to an upper limit of 1.4 TeV and effectively transforms the LHC into a Pomeron-Pomeron collider with variable center-of-mass energy. The visible cross-section for such a leading proton selection will be smaller, since the efficiency for the selection has been assumed to be 100 %. Requiring at least two jets (points) reduces the cross-section for small masses quite significantly and effectively suppresses masses below 100 GeV. For masses above 1.2 TeV, the cross-section is hardly reduced.

To study the sensitivity to the partonic structure of the Pomeron, different partonic distributions were used and the resulting shape of the pseudo-rapidity distribution of the two leading jets was investigated. In figure 11 (right part) the cross-section for hard central diffractive scattering with two leading protons and at least two jets is shown as a function of the jet pseudo-rapidity η_{jet}. A hard gluon distribution (dashed line) leads to a rather flat distribution in η_{jet}. For the case of a soft gluon and of the CKMT distribution, most jets are produced centrally.

The sample of single diffractive events generated with PHOJET corresponds to a fraction of 4×10^{-5} of the integrated luminosity (1 fb^{-1}) expected for one year running with a constant luminosity of 10^{32} cm^{-2} s^{-1}. This would give an expectation of 5×10^9 events (due to single diffractive scattering) with a leading proton and two jets ($|\eta| < 3.2$ and $E_T > 10$ GeV). Increasing the E_T cut in steps of 10 GeV would reduce the corresponding number of events by approximately one order of magnitude. This estimate however does not include any acceptance or efficiency for the leading proton detection and assumes also a specific running scenario, which is optimistic.

8 Topics and issues for further studies

Many more steps are needed to arrive at more quantitative results than the ones presented in this note. The possible studies can be separated into detector oriented investigations and physics oriented investigations.

In order to be able to obtain more realistic results, it is important to quantify the acceptance of Roman Pot detectors in a given configuration (position of the detectors), which could be taken as the one of the TOTEM proposal [67]. The acceptance (and the resolutions) should be determined as function of the variables ξ and t, for different assumptions on the value of the β^* at the interaction point (e.g. $\beta^* = 0.5$ m – normal conditions – and $\beta^* = 1000$ m – special optics). For the calculations, reasonable assumptions on the closest approach of the detectors to the beam (e.g. $K \cdot \sigma_{beam}$ with $K \approx 10 - 15$) and on the position resolution of the detectors will have to be made.

Furthermore, the capabilities of a proton momentum measurement using Roman Pot stations located before and after the first dipole magnet should be investigated. This should include the determination of the expected resolution in longitudinal momentum x_F, as a function of ξ and t.

In this context, possible running scenarios for measurements of diffractive scattering

should be developped and later on these conditions (together with estimates of the achievable integrated luminosity) should be used to quantify the expected statistical accuracy. One possibility is to foresee periods of dedicated running, at which the conditions are optimised for diffractive scattering studies, i.e. in most cases no pile-up events (this would limit the luminosity to values of about 10^{32} cm^{-2} s^{-1}). One of the main questions in this case is the achievable integrated luminosity without influencing the main physics programme of the LHC to be done at design luminosity. A second possibility would be to include trigger on diffractive scattering in the second half (forth quarter or similar) of a machine fill, where the conditions are more favourable than at the beginning of a fill.

As an alternative selection of diffractive scattering, the approach of large rapidity gaps in the forward direction (around the beam pipe) should be addressed. CDF and D0 make use of the multiplicity in terms of calorimeter towers and/or charged tracks and have observed excesses in the zero multiplicity bins, which are associated to diffractive scattering. These investigations have to take the geometry and performance of the ATLAS detector (for $|\eta| < 5$) into account and could be extended beyond $|\eta| = 5$ for possible additional detectors to be added to ATLAS. An important quantity for these studies is the upper limit on the mass of a colourless leading system, which does produce such a large rapidity gap signature. If this type of selection is to be used, a contamination from diffractive dissociation has to be taken into account.

Based on the conditions discussed previously, studies of hard diffractive scattering with various probes of the hard scattering process (jets, photons, W/Z bosons, heavy quarks, ...) should be used to derive the kinematic reach and the corresponding statistical accuracies for cross-section measurements, which potentially could be used to derive diffractive parton densities. Obviously, the kinematic reach will be crucially dependent of the lowest feasible thresholds for these objects at the trigger level, which have to be chosen large enough not to exhaust the available bandwidth. Based on these cross-section estimates, approaches to constrain or extract diffractive parton densities could be studied. This should include the theoretical question whether process independent diffractive parton densities can be at all obtained from diffractive scattering in hadron collisions.

Further studies are also needed to establish a scheme for an efficient trigger on these events, which should be based on the expected possible selection of such events by an offline analysis. For the first level trigger, several possibilities can be listed:

- A trigger based on a fast coincidence between various detector planes in a single Roman Pot, giving a track segment. To stay within the maximum allowed LVL1 latency of 2.5 μs, the actual time for doing the pattern recognitition giving the track segments has to be much smaller than this amount, as most of the time has to be used to transfer the signals from the Roman Pot detector locations to the central trigger processor (and to distribute the decision back to the frontend electronics).

- Using a forward energy trigger (which would sum e.g. the energy deposition over the full azimuth in the forward LAr calorimeter) to select events with a large rapidity gap signature. Such a trigger is possible within the present LVL1 calorimeter trigger design, studies however would have to be performed to demonstrate the possible effective usage.

- A trigger on jets (or photons or leptons from W/Z decays) with much lower thresholds than presently foreseen for inelastic proton-proton collisions.

In all these cases, the higher levels (LVL2 and EF) of the trigger system would have to apply additional criteria to reduced the rate to an acceptable value. It should be quantified what the expected statistical accuracy would be, when a reasonable assumption on the fraction of the LVL1 bandwidth allocated to this type of physics is made.

Related to a discussion of running scenarios is the investigation of possible background contributions, which could either fake the signature of a hard diffractive scattering event or could obscure the properties (esp. the large rapidity gap signature) of these events. The first issue would happen if a soft diffractive event occurs simultaneously with a non-diffractive event (pile-up), where the latter contains high p_T objects(e.g. jets) in the final state. This source of background is obviously directly dependent of the value of the luminosity. An example for the second class is the simultaneous occurrence of a hard diffractive scattering and a minimum bias event, where the latter possibly obscures the measurement of the diffractive event.

Besides these background sources mostly related to the luminosity conditions at LHC, also the background from other processes (like meson exchange or double diffractive dissociation) has to be taken into account. Further studies could include the use of different models (and MC implementation) for hard diffractive scattering.

9 Conclusions

This note summarizes first studies done within ATLAS on measurements of hard diffractive scattering at the LHC. These studies required the detection of leading protons as signature for diffractive scattering, together with the occurrence of jets as signature for a hard scattering process. They were restricted to the particle level without taking into account the effect of detector resolutions. First estimates of visible cross-sections and sensitivities to the underlying partonic structure were obtained.

As discussed in the previous sections, a whole bunch of further studies and investigations needs to be done in order to be able to quantify the possible results obtained from studies of hard diffractive scattering at LHC. This has to include studies on detector issues, such as the acceptance of Roman Pot detectors; discussions on possible running and triggering scenarios and theoretical investigations on the concept of diffractive parton densities in hadron collisions. Further related topics concern diffractive Higgs production (which could provide in central diffractive production a precise mass measurement using the recoil mass) and diffraction at very high t (probing the validity of predictions of perturbative QCD).

References

[1] R. Engel, PHOJET manual (1995) `http://lepton.bartol.udel.edu/~eng/phojet.html`.

[2] F.E. Low, Phys. Rev. D12, 163 (1975); S. Nussinov, Phys. Rev. Lett 34, 1286 (1975).

[3] V. N. Gribov, Sov. Phys. JETP **26**, 414 (1968).

[4] V. N. Gribov and A. A. Migdal, Sov. J. Nucl. Phys. **8**, 583 (1969).

[5] V. A. Abramovski, V. N. Gribov, and O. V. Kancheli, Sov. J. Nucl. Phys. **18**, 308 (1974).

[6] V. Innocente, A. Capella, and J. Trân Thanh Vân, Phys. Lett. **B213**, 81 (1988).

[7] K. Hahn and J. Ranft, Phys. Rev. **D41**, 1463 (1990).

[8] P. Aurenche *et al.*, Phys. Rev. **D45**, 92 (1992).

[9] A. Capella, U. Sukhatme, C. I. Tan, and J. Trân Thanh Vân, Phys. Rep. **236**, 225 (1994).

[10] A. B. Kaidalov, Phys. Rep. **50**, 157 (1979).

[11] A. B. Kaidalov and K. A. Ter-Martirosyan, Nucl. Phys. **B75**, 471 (1974).

[12] K. Goulianos, Phys. Rep. **101**, 169 (1983).

[13] D. Bernard *et al.*, Phys. Lett. **B166**, 459 (1986).

[14] S. Abachi *et al.*, Phys. Rev. Lett. **76**, 734 (1996).

[15] F. Abe *et al.*, Phys. Rev. Lett. **80**, 1156 (1998).

[16] W. Buchmüller, Phys. Lett. **B353**, 335 (1995).

[17] W. Buchmüller and A. Hebecker, Phys. Lett. **B355**, 573 (1995).

[18] A. Edin, G. Ingelman, and J. Rathsman, Phys. Lett. **B366**, 371 (1995).

[19] J. F. Amundson, O. J. P. Eboli, E. M. Gregores, and F. Halzen, Phys. Lett. **B372**, 127 (1996).

[20] O. J. P. Eboli, E. M. Gregores, and F. Halzen, (hep-ph/9708283) (unpublished).

[21] A. H. Mueller and W. K. Tang, Phys. Lett. **B284**, 123 (1992).

[22] V. Del Duca and W. K. Tang, Phys. Lett. **B312**, 225 (1993).

[23] R. Engel, Z. Phys. **C66**, 203 (1995).

[24] R. Engel and J. Ranft, Phys. Rev. **D54**, 4244 (1996).

[25] F. W. Bopp, R. Engel, D. Pertermann, and J. Ranft, Phys. Rev. **D49**, 3236 (1994).

[26] B. L. Combridge, J. Kripfganz, and J. Ranft, Phys. Lett. **B70**, 234 (1977).

[27] D. W. Duke and J. F. Owens, Phys. Rev. **D26**, 1600 (1982).

[28] R. Engel, M. A. Braun, C. Pajares, and J. Ranft, Z. Phys. **C74**, 687 (1997).

[29] J. L. Cardy, Nucl. Phys. **B75**, 413 (1974).

[30] A. B. Kaidalov, L. A. Ponomarev, and K. A. Ter-Martirosyan, Sov. J. Nucl. Phys. **44**, 468 (1986).

[31] A. Capella, A. Kaidalov, C. Merino, and J. Trân Thanh Vân, Phys. Lett. **B343**, 403 (1995).

[32] A. Capella *et al.*, Phys. Rev. **D53**, 2309 (1996).

[33] J. Collins, L. Frankfurt, and M. Strikman, Phys. Lett. **B307**, 161 (1993).

[34] J. C. Collins *et al.*, Phys. Rev. **D51**, 3182 (1995).

[35] B. Kniehl, H.-G. Kohrs, and G. Kramer, Z. Phys. **C65**, 657 (1995).

[36] R. Engel and J. Ranft, to appear in Proceedings of The Int. Symposium on Near Beam Physics, Fermilab, Sept. 22-24, 1997 (unpublished).

[37] B. Abbott *et al.*, Fermilab–Conf–97/250–E (unpublished).

[38] J. C. Collins, Phys. Rev. **D57**, 3051 (1998).

[39] G. Ingelman, presented at this meeting (unpublished).

[40] J. D. Bjorken, Phys. Rev. **D47**, 101 (1993).

[41] F. W. Bopp, R. Engel, J. Ranft, and A. Rostovtsev, to appear in Proceedings of the International Symposium on Photon Interactions and Photon Structure (PHOTON '97), Egmond aan Zee, The Netherlands (unpublished).

[42] J. W. Chapmann *et al.*, Phys. Rev. Lett. **32**, 257 (1974).

[43] J. Schamberger *et al.*, Phys. Rev. Lett. **34**, 1121 (1975).

[44] M. G. Albrow *et al.*, Nucl. Phys. **B108**, 1 (1976).

[45] J. C. M. Armitage *et al.*, Nucl. Phys. **B194**, 365 (1982).

[46] R. E. Ansorge *et al.*, Z. Phys. **C33**, 175 (1986).

[47] D. Robinson and C. E. Wulz, report UA1-TN / 89-10 (unpublished).

[48] N. A. Amos *et al.*, Phys. Lett. **B243**, 158 (1990).

[49] N. A. Amos *et al.*, Phys. Lett. **B301**, 313 (1993).

[50] F. Abe *et al.*, Phys. Rev. **D50**, 5535 (1994).

[51] K. H. Streng, Phys. Lett. **166B**, 443 (1986).

[52] M. Bozzo *et al.*, Phys. Lett. **B147**, 392 (1984).

[53] D. Bernard *et al.*, Phys. Lett. **B186**, 227 (1987).

[54] A. Brandt *et al.*, Phys. Lett. **B297**, 417 (1992).

[55] R. Engel, J. Ranft, and S. Roesler, Phys. Rev. **D52**, 1459 (1995).

[56] T. Ahmed *et al.*, Nucl. Phys. **B435**, 3 (1995).

[57] S. Aid *et al.*, Z. Phys. **C69**, 27 (1995).

[58] M. Derrick *et al.*, Phys. Lett. **B346**, 399 (1995).

[59] M. Derrick *et al.*, Phys. Lett. **B356**, 129 (1995).

[60] M. Derrick *et al.*, Z. Phys. **C67**, 227 (1995).

[61] F.W.Bopp, R.Engel, J.Ranft "Rapidity Gaps and the Phojet Monte Carlo", hep-ph/9803437, Talk presented by J. Ranft at the LAFEX International School of High Energy Physics, Session C: Workshop on diffractive physics LISHEP98, Rio de Janeiro, Feb. 16-20 1998. Also Siegen Univeristy preprint Si 98-25 and Bartol Research Fondation Preprint BA-98-17

[62] M. Albrow, Fermilab–Conf–97/362 (unpublished).

[63] F. Abe *et al.*, Phys. Rev. Lett. **79**, 2636 (1997).

[64] F. Abe et al., Phys. Rev. Lett. 79 (1997) 2636.

[65] CDF collaboration (M.G. Albrow, for the collaboration), 'Diffractive Dijet Production in CDF', preprint FERMILAB-CONF-98-134-E (1998).

[66] Code based on the CONE algorithm by I.C. Park, IFAE-UAB Barcelona, developed for the JADE experiment.

[67] TOTEM collaboration, Technical Proposal (1999).

A Details of The Model

The realization of the DPM in PHOJET [23, 24] with a hard and a soft component is similar to the event generator DTUJET [8, 25] for p–p and $\bar{p}$–p collisions. Interactions of hadrons are described in terms of reggeon ($I\!R$) and pomeron ($I\!P$) exchanges. The pomeron exchange is artificially subdivided into *soft* processes and processes with at least one large momentum transfer (*hard* processes). This allows us to use the predictive power of the QCD-improved Parton Model with lowest-order QCD matrix elements [26,27] and parton distribution functions (PDFs). Practically, soft and hard processes are distinguished by applying a transverse momentum cutoff $p_\perp^{\rm cutoff}$ of about 3 GeV/c to the scattered partons. The pomeron is considered as a two-component object with the Born graph cross section for pomeron exchange given by the sum of hard and soft cross sections.

High-mass diffraction dissociation is described in the following way. In order to get an efficient parametrization of the Born graph cross sections describing diffraction within Gribov's reggeon calculus, the triple-, loop- and double-pomeron graphs shown in Fig. 12 are calculated using a renormalized pomeron intercept $\alpha_{I\!P} = 1 + \Delta_{I\!P} = 1.08$. The corresponding formulae are given in [28].

Shadowing corrections are approximated by unitarizing the enhanced graphs together with the leading one-pomeron exchange (including soft and hard contributions) in a *"two-channel eikonal model"* [8, 23, 24].

In case of diffractive multiparticle production, in addition to the shadowing contribution from multiple pomeron exchange between projectile and target, also rescattering

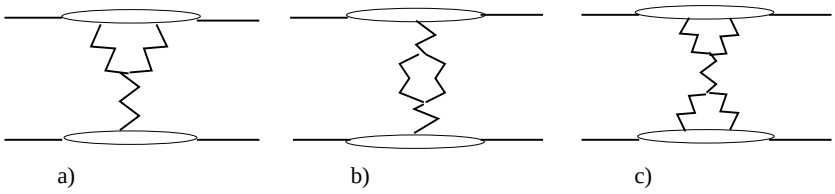

Figure 12: Enhanced pomeron exchange graphs considered in the model: a) triple-pomeron, b) loop-pomeron, and c) double-pomeron graphs. The zig-zag lines represent pomeron propagators.

effects in pomeron-hadron and pomeron-pomeron interactions have to be considered. For the calculation of particle production, it is assumed that the pomeron-pomeron coupling can be described by the formation of an intermediate hadronic system $h^\star$ the pomerons couple to, following refs. [29, 30]. Assuming that this intermediate hadronic system has properties similar to a pion, the n-m pomeron coupling g_{n-m} reads [30]

$$g_{n-m} = G \prod_{i=1}^{n+m-2} g_{h^\star I\!P} \tag{9}$$

with $g_{h^\star I\!P} = g_{\pi I\!P}$ being the pomeron-pion coupling. G is a scheme-dependent constant. Hence, pomeron-hadron and pomeron-pomeron scattering are expected to exhibit features similar to pion-hadron and pion-pion scattering, respectively.

To introduce hard interactions in diffraction dissociation, the impact parameter amplitude of the exchanged (renormalized) pomerons in pomeron–hadron and pomeron–pomeron scattering is again interpreted as the eikonalized amplitude of soft and hard interactions

$$a_{AI\!P}(M_{\rm D}, \vec{B}) \approx \frac{i}{2}\, G\, \left\{1 - \exp\left[-\chi_{\rm S}^{\rm diff}(M_{\rm D}, \vec{B}) - \chi_{\rm H}^{\rm diff}(M_{\rm D}, \vec{B})\right]\right\}\ . \tag{10}$$

The diffractive eikonal functions for the soft nad hard part are respectively:

$$\chi_{\rm S}^{\rm diff}(M_{\rm D}, \vec{B}) = \frac{g^0_{AI\!P} g^0_{h^\star I\!P} (M_D^2/s_0)^{\Delta_{I\!P}}}{8\pi b_{I\!P}(M_D^2)} \exp\left(-\frac{\vec{B}^2}{4b_{I\!P}(M_D^2)}\right) \tag{11}$$

$$\chi_{\rm H}^{\rm diff}(M_{\rm D}, \vec{B}) = \frac{\sigma_{\rm hard}^{AI\!P}(M_D^2)}{8\pi b_{\rm h,diff}} \exp\left(-\frac{\vec{B}^2}{4b_{\rm h,diff}}\right), \tag{12}$$

where $\sigma_{\rm hard}^{AI\!P}$ is the parton model cross section for hard pomeron–A scattering (A can be a hadron, photon or pomeron). In all calculations the pomeron PDFs proposed by Capella, Kaidalov, Merino, and Tran (CKMT) [31, 32] with a hard gluon component are used.

To estimate the sensitivity of the model results to non-factorizing coherent pomeron contributions as proposed in [33, 34], a toy model with a direct pomeron-quark coupling [35] can be optionally used. In this case, the pomeron is treated similar to a photon having a flavor independent, unknown quark coupling λ. The corresponding matrix elements are given in [36].

Both the CDF and D0 collaborations have found dijet production by color–singlet exchange [14, 15]. These Jet–gap–Jet (JgJ) events are not due to traditional diffractive

processes. The two jets separated by a rapidity gap are in polar angle back–to–back correlated. Certainly in double–diffractive events, describing the diffractively produced systems on both sides of the gap by pomeron–hadron scattering, jets are also found, but these jets would not be back–to–back correlated. Therefore, these events have to be considered as mainly due to a new mechanism of hard pomeron exchange.

To describe these events within the PHOJET Monte Carlo, SCR has been introduced between hard scattered partons in nondiffractive events following Eboli, Gregores and Halzen [20]. This mechanism is quite similar to the the soft color interaction mechanism described by Ingelman [39]. The following SCR probabilities [20] in PHOJET are used:

$$F_{qq} : F_{qg} : F_{gg} = \frac{1}{9} : \frac{1}{24} : \frac{1}{64}. \tag{13}$$

The simplest hard q–q event, where SCR leads to a large rapidity gap between two jets is an event with just one single hard valence–quark – valence–quark scattering. According to the Dual Parton Model, two color strings are considered in normal events. Each string is stretched between one scattered quark and the diquark of the other hadron, and no large rapidity gap is present in such events. In events with SCR, the color reconnection comes from the exchange of soft gluons. Now the color strings connect the hard scattered quark and the diquark of the same hadron, and these are events with a large rapidity gap.

As another example, the simplest hard g–g event where SCR leads to a large rapidity gap between two jets is an event with just one hard g–g scattering. In normal events two color strings are again obtained. They connect the (soft) valence quark of one hadron via the hard scattered gluon to the (soft) diquark of the other hadron. In events with SCR the color strings are stretched from the (soft) valence quark of one hadron via one hard scattered gluon to the (soft) diquark of the same hadron. Such events might have a large rapidity gap.

In most of events, multiple soft and hard interactions are produced, and even if a large rapidity gap appears in one of the multiple collisions, the gap might be filled by hadrons resulting from the other collisions. The Monte Carlo simulation of complete events incorporates this effect, in this way PHOJET accounts already for the gap survival probability [40, 41].

B Comparing hadron production in diffractive processes to non-diffractive particle production in p–p and γ–γ reactions

In Fig. 13.a the jet transverse energy distributions in p–p and γ–γ collisions are compared with the ones in $I\!P$–$I\!P$ collisions. In the channels with pomerons the results according to the full model are reported together with those without multiple interactions and those with a direct pomeron–quark coupling. In all non-diffractive collisions $\sqrt{s} = 100$ GeV and the diffractive events are generated in $\sqrt{s} = 2$ TeV collisions with $M_D = 100$ GeV/c^2. The differences in the jet transverse energy distributions between the channels are, as expected, more pronounced than in the hadron $p_\perp$ distributions. An important reduction in the jet distributions in the model without multiple interactions can be observed. The effect of the direct pomeron coupling is as dramatic as the effect due to the direct photon

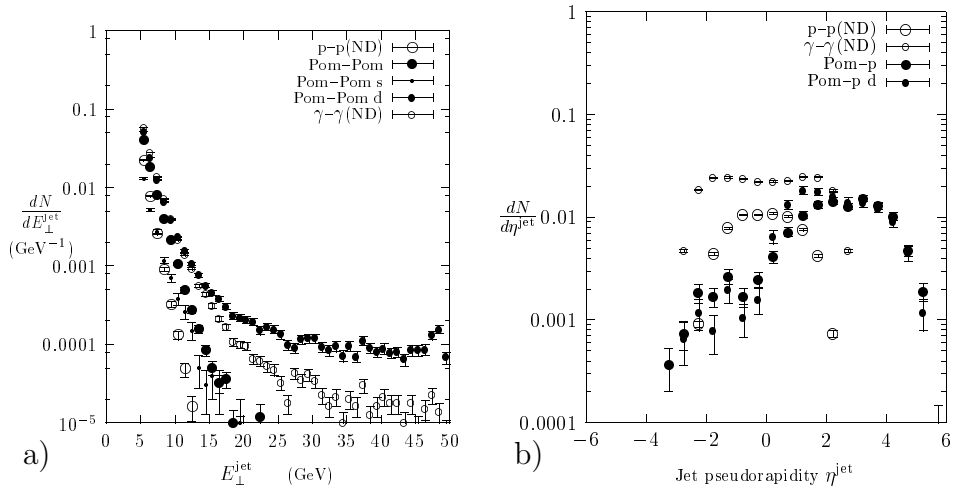

Figure 13: (a) Jet transverse energy distributions in non-diffractive p–p and γ–γ collisions compared with the jet transverse energy distribution in central diffraction (pomeron–pomeron collisions). For the latter channel we give the distributions separately for the full model, the model without multiple interactions (s) and the model with a direct pomeron coupling (d). The distributions were generated with PHOJET, the c.m. energy / diffractive mass is 100 GeV in all cases. (b) Jet pseudorapidity distributions in non-diffractive p–p and γ–γ collisions compared with the jet pseudorapidity distribution in single diffraction (pomeron–p scattering). The distributions were generated with PHOJET, again the c.m. energy / diffractive mass is 100 GeV in all cases, but the pseudorapidities in the collisions with pomerons given refer to the $\sqrt{s} = 2$ TeV p–p collisions used to generate the diffractive events.

coupling. The $E_\perp$ distributions in the $I\!P$–γ and $I\!P$–$I\!P$ channels extend up to the kinematic boundary. In the latter two cases, as in the case of γ–γ collisions, the entries at large $E_\perp$ come only from direct processes.

In Fig. 13.b jet pseudorapidity distributions in p–p, γ–γ and $I\!P$–p are reported. Again, all collisions are at $\sqrt{s} = 100$ GeV with the diffractive events generated in $\sqrt{s} = 2$ TeV collisions. Substantial differences in the shape of the pseudorapidity distributions can be observed for jets.

C More comparisons of the PHOJET results with data

C.0.4 Diffractive cross sections

In Fig. 14.a data on single diffractive cross sections [42–50] are compared with PHOJET results ($M_{\rm D}^2 < 0.05s$). It has to be noticed that the data on single diffractive cross sections at collider energies are subject to large uncertainties. Nevertheless the rise of the cross section from ISR energies to the energies of the CERN and FERMILAB colliders is less steep than expected from the Born level expression, which is the triple pomeron formula.

In Fig. 14.b the central diffraction cross sections in proton-proton collisions, from PHOJET is compared with the cross section calculated by Streng [51]. While in PHOJET

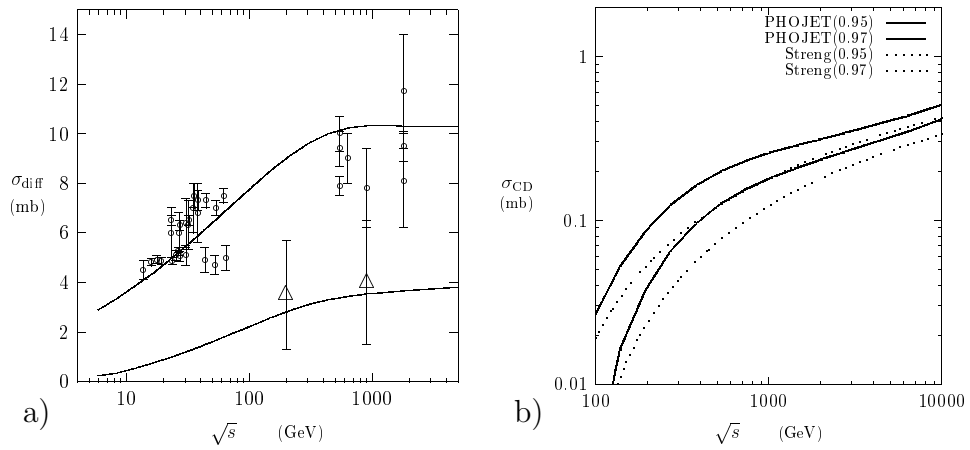

Figure 14: (a) Single and double diffractive $p - \bar{p}$ cross sections as a function of the center of mass energy $\sqrt{s}$. Model results are compared to data on single diffractive cross sections [42–50]. In addition, some experimental estimates for the cross section on double diffraction dissociation [46, 47] are shown (triangles). (b) The energy dependence of the central diffraction cross section. We compare the cross section as obtained from PHOJET with unitarization using a supercritical pomeron with the cross section obtained by Streng [51] without unitarization and with a critical pomeron. Both cross sections are for the same two kinematic cuts: $M_{\rm CD} > 2$ GeV/c^2 and Feynman-x of the scattered hadron $x_F > 0.95$ (upper curves) and 0.97 (lower curves).

a supercritical pomeron with $\Delta_{\tilde{I\!P}} = 0.08$ is adopted, Streng [51] uses a critical Pomeron with $\Delta_{I\!P} = 0$. It can be remarked that also the double-pomeron cross section grows in Born approximation with s like $\sim s^{2\Delta_{\tilde{I\!P}}}$. This rapid increase is damped in PHOJET by the unitarization procedure. At high energies, contributions from multiple interactions become important. The rapidity gaps are filled with hadrons due to inelastic rescattering and the cross section for central diffraction gets strongly reduced. In contrast, Streng calculates only the Born term cross section.

C.1 Diffractive hadron- and jetproduction

Different experiments have studied hadron production in single diffraction dissociation. Among the others, the following results can be mentioned for the test of PHOJET.

1. In Figs. 15 and 16 data from the UA–4 Collaboration [13, 52, 53] are reported. A reasonable agreement with PHOJET is observed. In particular, besided the results obtained with the full model, also the contribution from one pair of chains only (single interaction model) is shown. This is what is expected from the Born term without the contributions from hard diffraction (minijets) and multiple soft interactions. It is evident from the data as well as from the model that multiple interactions and minijets lead to a rising rapidity plateau in pomeron–proton collisions in a similar way as observed in hadron–hadron collisions.

2. Hard diffractive proton–antiproton interactions were investigated by the UA–8 Collaboration [54]. In this experiment the existence of a hard component of diffraction

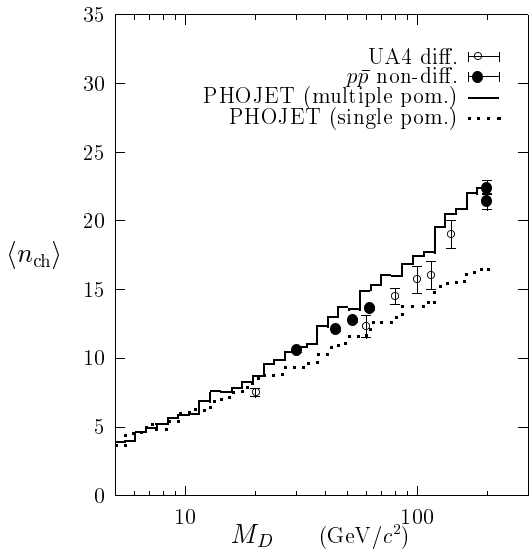

Figure 15: Mean charged particle multiplicity of the diffractively produced hadronic system with invariant mass M. UA–4 data [13] are compared to single and multiple interaction model predictions and data on non-diffractive $p\bar{p}$ interactions at $\sqrt{s} = M$.

was demonstrated for the first time. A satisfactory comparison of the consistency of PHOJET with the results of this experiment is reported in Ref. [55]

Results on single photon diffraction dissociation and in particular hard single diffraction were presented by both experiments at the HERA electron–proton collider [56–60].

In particular, the ZEUS Collaboration [59] has presented differential and integrated jet pseudorapidity cross sections for jets with $E_T^{\rm jet} > 8$ GeV, giving an absolute normalization of these data. This allows one a more severe check of the model. In Figs. 17 the differential jet pseudorapidity cross sections from ZEUS is compared to the model. The Monte Carlo events from PHOJET have been treated with the same cuts and trigger as used for the data. A reasonable agreement is found although it must be pointed out how the data include contributions from non-diffractive processes while MC calculations concern only diffractive events.

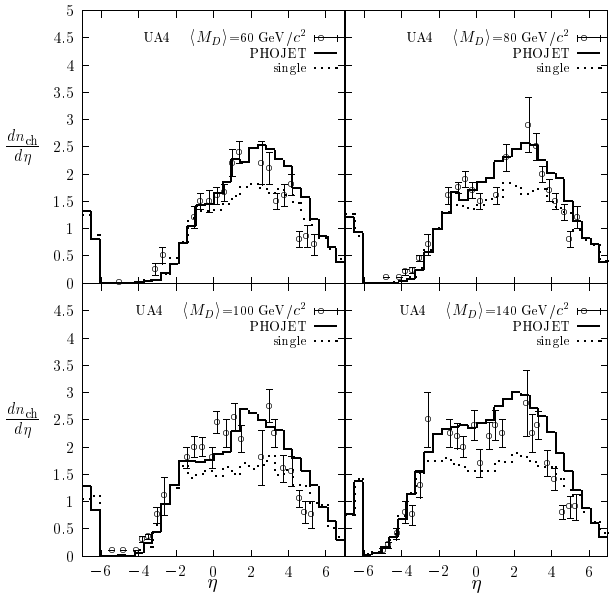

Figure 16: Pseudorapidity distribution of charged hadrons in single diffraction dissociation. UA–4 data [13] to model predictions.

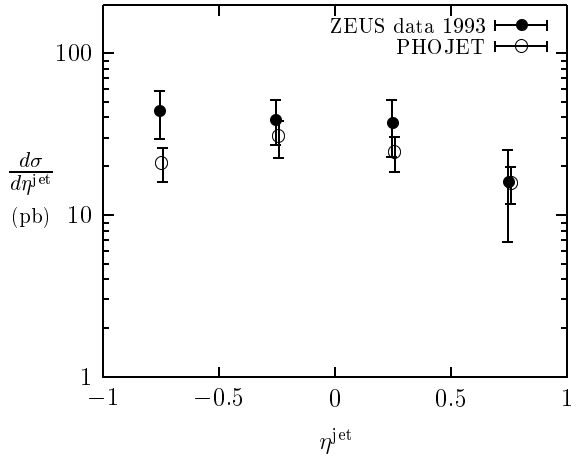

Figure 17: Differential $e-p$ cross section $d\sigma/d\eta_{\rm jet}(\eta^{had}_{max} < 1.8)$ for inclusive jet production with $E_T^{\rm jet} > 8$ GeV in the kinematic region $Q^2 \leq 4$ GeV^2 and $0.2 < y < 0.85$. We compare data from the ZEUS Collaboration [59] with PHOJET results using the same trigger as used for the ZEUS data.